Structure and Dynamics of the Human Granulocyte Colony-Stimulating Factor Determined by NMR Spectroscopy. Loop Mobility in a Four-Helix-Bundle Protein[†,‡]

Thomas Zink,[§] Alfred Ross,[§] Kai Lüers,[§] Christian Cieslar,[§] Rainer Rudolph,[∥] and Tad A. Holak*[,§]

Max-Planck-Institut für Biochemie, D-82152 Martinsried, F.R.G., and Boehringer-Mannheim GmbH, Biochemical Research Center, D-82377 Penzberg, F.R.G.

Received March 2, 1994; Revised Manuscript Received April 26, 1994[⊗]

ABSTRACT: Recombinant ^{15}N- and ^{13}C-labeled human granulocyte colony-stimulating factor (rh-metG-CSF) has been studied by 2D and 3D NMR using uniformly labeled protein, as well as residue-specific ^{15}N-labeled samples. Assignment of 90% of the backbone resonances and 85% of side-chain resonances has enabled the determination of both the secondary and tertiary structures of the protein. The fold is similar to those of the human growth hormone and other growth factors. Four stretches of helices were identified between residues 11 and 41 (helix A), 71 and 95 (helix B), 102 and 125 (helix C), and 145 and 170 (helix D), which form a left-handed four-helix bundle with helices A and B aligned parallel to one another (up–up) and antiparallel to helices C and D (down–down). An additional short fifth helix (E) is part of the AB loop connecting helices A and B. Examination of the protein's relaxation behavior, based on the model-free approach of Lipari and Szabo, shows that the G-CSF backbone has a well-defined structure of limited conformational flexibility in helices. In contrast, the long loop connecting helices C and D exhibits substantial fast internal motion compared to the overall rotational correlation time of the whole molecule, which is on the order of 13 ns.

Human granulocyte colony-stimulating factor (rh-metG-CSF[1]), a 174-residue protein (MW = 18 800, p*I* = 6.1), belongs to a group of glycoproteins called hematopoietic colony-stimulating factors (Nomura et al., 1986). Other important members in this group are macrophage colony-stimulating factor (M-CSF), granulocyte–macrophage colony-stimulating factor (GM-CSF), the interleukins (IL-2 to IL-7), erythropoietin (EPO), and growth hormone (GH). All of these proteins are present in the blood at picomolar concentrations and play an important role in the process of blood formation. They are involved in the constant replenishment of the usually short-lived unicellular components of blood and also participate in immunological defense reactions (Metcalf, 1986; Clark & Kamen, 1987). Elevated expression of these proteins is induced in the bone marrow, monocytes, fibroblasts, endothelial cells, and T-cells (Kirchner et al., 1993; Clark & Kamen, 1987) in response to inflammatory mediators, such as lipopolysaccharides from bacteria. Different growth factors differ in their specificities for different progenitor cell types (Clark & Kamen, 1987; Kaushansky, 1992). G-CSF and M-CSF influence late progenitor cells that have already undergone some kind of differentiation and specifically lead to the proliferation of granulocytes (Metcalf et al., 1983) and macrophages (Stanley et al., 1977), respectively.

G-CSF has four major functions: it is required for the survival of hematopoietic progenitor cells, it induces proliferation of the precursor cells, and it is responsible for their differentiation into mature neutrophilic granulocytes and for the activation of mature neutrophilic granulocytes (Morstyn & Burgess, 1988). G-CSF-induced host defense mechanisms include phagocytosis and cytotoxicity by increased production of superoxide anions by mature neutrophils in the presence of the bacterial peptide f-Met-Leu-Phe, for example (Clark & Kamen, 1987; Nagata, 1989). The sugar chain present in the native protein (linked to Thr-133-$^{\gamma}$O; Kubota et al., 1990) is not required for biological activity, since recombinant G-CSF without the carbohydrate moiety exhibits the same activity (Oheda et al., 1990; Souza et al., 1986), but is presumed to stabilize the protein against thermal denaturation.

A person exhibiting a low titer of neutrophils (which account for the major part of the granulocytes) is likely to suffer from infections. This state, called neutropenia, can result from chemotherapy in the course of cancer treatment (Crawford et al., 1990), after bone marrow transplants (Molineux et al., 1990), and in AIDS cases (Clark & Kamen, 1987; Glaspy et al., 1989). In such cases, some means of elevating the level of neutrophils is required. G-CSF is one potential candidate for this purpose (Scarffe & Kamthan, 1990; Glaspy & Golde, 1992; Gabrilove, 1992) and has been in clinical use since 1991. Other growth factors have also been tested in this respect (Clark & Kamen, 1987).

While there is no significant sequence homology between G-CSF and other hematopoietic proteins, except for IL-6 (32%) (Bazan, 1991), they all share a common backbone fold

[†] This work was supported by research grants from the Deutsche Forschungsgemeinschaft.

[‡] Coordinates have been deposited in the Brookhaven Protein Data Bank under the file name 1GNC.

[§] Max-Planck-Institut für Biochemie.

[∥] Boehringer-Mannheim GmbH.

[⊗] Abstract published in *Advance ACS Abstracts,* June 1, 1994.

[1] Abbreviations: rh-metG-CSF, human granulocyte colony-stimulating factor; G-CSF, granulocyte colony-stimulating factor; M-CSF, macrophage colony-stimulating factor; MG-CSF, macrophage–granulocyte colony-stimulating factor; IL, interleukin; EPO, erythropoietin; GH, growth hormone, rmsd, root mean square difference; NMR, nuclear magnetic resonance; NOE, nuclear Overhauser effect; NOESY, two-dimensional NOE spectroscopy; TOCSY (HOHAHA), total correlation spectroscopy (homonuclear Hartmann–Hahn spectroscopy); 2D, two-dimensional; 3D, three-dimensional; HNCA, amide proton to nitrogen to α-carbon correlation; TPPI, time proportional phase incremenataion; τ_m, overall rotational correlation time; S^2, order parameter; τ_e, effective correlation time for internal motion; R_{ex}, exchange line width; T_1, longitudinal relaxation time; T_2, transverse relaxation time.

0006-2960/94/0433-8453$04.50/0

(Vos et al., 1992; Diederichs et al., 1991; Mc Kay, 1992; Smith et al., 1992). The first structure to be solved for a protein of this family was that of the human growth hormone (de Vos et al., 1992). It is a four-helix bundle with an up–up–down–down alignment of helices rather than an up–down–up–down one. This backbone fold has also been observed in macrophage colony-stimulating factor (Pandit et al., 1992), granulocyte–macrophage colony-stimulating factor (Walter et al., 1992), and human interleukin 4 (Smith et al., 1992; Powers et al., 1992).

We have undertaken to elucidate the three-dimensional structure of G-CSF in solution by NMR spectroscopy. Recently, we presented the ^1H and ^{15}N resonance assignments of G-CSF and its secondary structure (Zink et al., 1992). In this article, we focus on the determination of the three-dimensional structure and the characterization of the backbone dynamics of G-CSF.

MATERIALS AND METHODS

Sample Preparation. Uniformly ^{15}N- and ^{15}N,^{13}C-labeled rh-metG-CSF was expressed in *Escherichia coli* strain TG1 in minimal medium (Riesenberg et al., 1990) and purified by the procedure described by Rudolph et al. (1990). Rh-metG-CSF samples specifically labeled with [^{15}N]glycine, [^{15}N]-serine, [^{15}N]leucine, [^{15}N]valine, [^{15}N]alanine, and [^{15}N]-lysine were produced in *E. coli* strain C600+ in a supplemented minimal medium (Senn et al., 1987) and purified as described previously (Zink et al., 1992). [3,5-$^2H_2$]Phe-rh-metG-CSF was prepared using an analogous procedure. The samples were typically 1–2 mM in protein and 50–60 mM in sodium phosphate, after the addition of 0.5 mL of H_2O/D_2O (90:10) or 0.5 mL of D_2O to the lyophilized powder and adjustment of the pH to 3.5. This low pH value was necessary due to the low solubility of rh-metG-CSF at higher pH values.

NMR Spectroscopy. All spectra were recorded at 27 °C on a Bruker AMX 600 spectrometer equipped with a multichannel interface and a BGU 10A gradient unit. A series of 2D and 3D double- and triple-resonance spectra was recorded. The double-resonance experiments were recorded with a broadband probehead tuned for nitrogen; for the triple-resonance experiments, the ^1H, ^{13}C, ^{15}N triple-resonance probehead was used. The gradient-enhanced heteronuclear NOE measurements were carried out with a self-shielded triple-resonance probe. Nuclear Overhauser enhancement spectroscopy (NOESY) experiments (Bodenhausen et al., 1984) were recorded with a pulse sequence in which the last 90° pulse was replaced by a jump–return sequence to suppress the water resonance (Plateau & Gueron, 1982). A homospoil pulse of 8 ms during the mixing time of 100 ms was also used. A total of 4096 complex data points was acquired in t_2 with a spectral width of 11.1 ppm in the F_2 dimension; in t_1, 750 increments were collected, and 192 scans per increment were accumulated. Quadrature detection in the indirectly detected dimensions was obtained with the TPPI method (Marion & Wüthrich, 1983). All 3D NMR spectra were processed on a Convex 220 with our in-house software, CC-NMR (Cieslar et al., 1993).

For the 3D heteronuclear spectra, the ^1H carrier frequency was placed at the water resonance in dimensions for which the whole proton sweep width of 11.1 ppm was acquired. In the ^{15}N-filtered proton dimension, where only the amide region was recorded, the carrier frequency was placed at 8.0 ppm. The minimum sweep width for covering the amide region of the proton spectrum was set to 5.75 ppm to position the residual signal of water outside the spectral region of interest. The

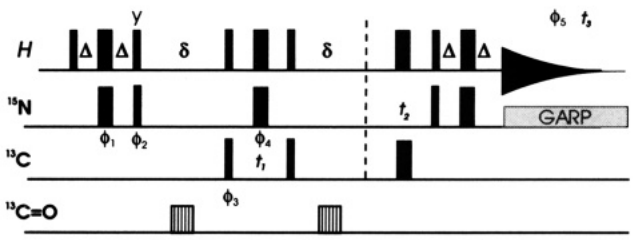

FIGURE 1: Pulse sequence for the HNCA experiment.

nitrogen carrier frequency was placed in the center of the backbone amides at 111 ppm (with respect to the frequency of liquid ammonia); the sweep width in this dimension was 41 ppm. For the triple-resonance HNCA experiment, the carrier frequency for carbon was at the center of the α-carbon region at 50 ppm with respect to TMS. To encompass the whole chemical shift range of α-carbons, the sweep width was set to 35.2 ppm. For all experiments that involved coupling constants to ^{15}N, the nitrogen was decoupled during acquisition by the GARP sequence (Shaka et al., 1983) with a field strength of 1 kHz. Presaturation of water was achieved with a field strength of 70 Hz with 1.3-s duration. The proton 90° hard pulse was determined to be 12 μs, the carbon 90° pulse had a length of 15 μs, and the nitrogen pulse was 18 μs. For the gradient probehead, the ^{15}N 90° pulse was set at 30 μs. Phase sensitivity in the acquisition dimension was achieved with the Bruker qsim mode, thus recording complex data points. Along all other dimensions TPPI was used for obtaining phase-sensitive spectra (Marion & Wüthrich, 1983).

A 2D heteronuclear multiquantum coherence (HMQC) ^1H–^{15}N correlation spectrum was acquired with standard methods (Summers et al., 1986). The 3D ^{15}N-separated NOESY–HMQC, with a mixing time of 120 ms including a homospoil (Zuiderweg & Fesik, 1990; Messerle et al., 1989), and TOCSY–HMQC (Marion et al., 1989) spectra with mixing times of 70 and 40 ms and 16 scans per t_1,t_2 pair were recorded. The size of the matrices was 176 × 64 × 1K data points. The MLEV-17 sequence (Bax & Davis, 1985), embraced by two hard spin–lock pulses of 1.5 ms for the removal of orthogonal coherences, was used in the TOCSY–HMQC experiment, and the TOCSY sequence was acquired in a clean TOCSY manner to avoid ROESY peaks (Griesinger et al., 1988). The seventeenth pulse of the MLEV sequence had a flip angle of 60°. The proton carrier frequency was placed between those of the amide and α-proton resonances at 5.9 ppm. To prevent sample heating, the power of the MLEV pulses was reduced by 6 dB compared to the hard pulses used outside the MLEV-17 scheme.

In a 3D triple-resonance ^NH–^{15}N–$^{13}C^\alpha$ HNCA measurement (Ikura et al., 1990; Kay & Bax, 1990), the pulse sequence of Ikura et al. (1990) was modified in the following manner. For the decoupling of the $^{13}C^\alpha$–$^{13}C^{C=O}$ coupling constant, the off-resonance refocusing 180° pulses at positions indicated in Figure 1 were used. Each pulse was designed as an off-resonance Dante sequence (Kay et al., 1990) built of 36 short pulses that were phase shifted with respect to each other by 30°. To achieve excitation at the off-resonance frequency of +18.4 kHz, each pulse had a length of 4.5 μs. The power setting of the amplifier was determined by a series of one-dimensional forward carbon spectra, consisting of the off-resonance pulse followed by a 90° excitation hard pulse. A homospoil between the soft and hard pulses was used in order to remove the off-resonance effects of the hard pulse. The power setting of the soft compared to the hard pulses was –13 dB. The duration of the delay Δ for transferring magnetization

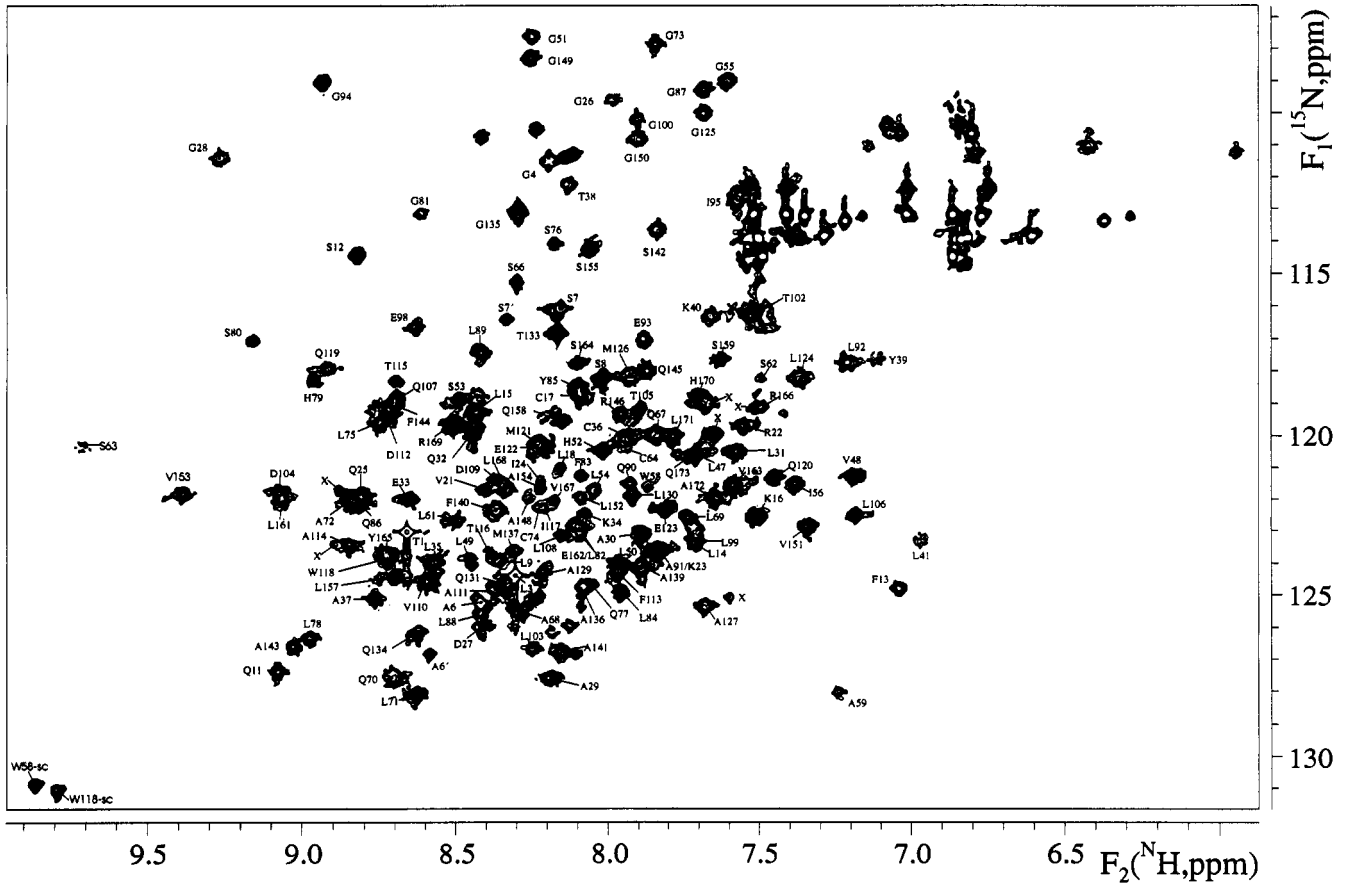

FIGURE 2: HMQC spectrum of uniformly labeled [^{15}N]rh-metG-CSF.

from nitrogen to α-carbon was optimized by a series of 1D experiments to be 25 ms. The δ delay of 2.4 ms was used in the ^{15}N HSQC type blocks of the sequence. For the excitation of α-carbons, a pulse with an excitation null in the carbonyl region was used, with a length of 60 μs and the power reduced by 10 dB compared to the full power of the amplifier. The size of the data matrix was 64 × 64 × 2K data points. A total of 48 scans was acquired, resulting in a total measurement time of 80 h. The spectrum was processed using linear prediction up to 128 data points along t_1 and t_2 to a final size of 128 × 128 × 1K data points. In all dimensions, Gaussian windows were applied. For water suppression, in all three-dimensional experiments presaturation was used.

Measurements of the ^{15}N relaxation times were performed according to the method of Kay et al. (1988), with a modification that minimizes the influences of the spectrometer instability on the amplitudes of the measured peaks. This modification consists of recording all relaxation delays for each of the 184 t_1 increments (by incrementing t_1 in an outer loop of the pulse program). The relaxation delays were 7.5, 30, 60, 120, 240, 480, and 961 ms and 7, 28, 49, 77, 112, 154, and 196 ms for the T_1 and T_2 experiments, respectively. The spectra were processed with cosine and Gaussian windows along t_1 and t_2, respectively, to the size of 256 × 2K data points. The transfer delay of the INEPT type blocks in the sequence was set to 2.4 ms. The pulse sequence for measuring the heteronuclear NOE is a modification of a scheme proposed by Ross et al. (1993a). Because of the broad line widths of ^{15}N signals of G-CSF (8 Hz), the constant time delay in the original pulse sequence was replaced by an evolution time t_1, incremented in a standard manner and followed by a refocused INEPT block. Gradient pulses were used both for coherence selection and for water suppression (Freund et al., 1994). Each gradient had the shape of a sine function 1 ms in length. No further delays were included in the sequence, thus avoiding large phase errors in the final spectra.

To achieve phase sensitivity along F_1, two data sets were recorded with alternating signs of the first (defocusing) gradient for each experiment. The processing of such experiments to a phase-sensitive data set, according to the method of States et al. (1982), is described by Ross et al. (1993b). To extract heteronuclear NOEs two measurements were performed: the first spectrum was taken with a broadband presaturation of protons, thus achieving the NOE enhancement, while the second spectrum (reference spectrum) was without the presaturation. A sequence of 120° pulses spaced by 10 ms, applied for a duration of 3 s, was used to achieve a steady-state broadband presaturation on all amides. A series of 1D experiments showed that after this time, all amide protons were saturated to 99%. The relaxation delay between the scans in the reference experiment had the same length as the total presaturation sequence to ensure the same equilibrium state. Processing parameters were identical to those in the spectra used to measure relaxation times.

Extraction of the T_1 and T_2 Times and NOEs. Intensities of the cross peaks in the T_1, T_2, and NOE spectra were obtained from the peak heights. T_1 and T_2 were calculated by fitting the function $[a \exp(t/T_{1,2})]$ to the data values. To minimize the mean square differences between the experimental intensities, d_i, and the fit function $[E(T_{1,2}) = \sum(d_i - a \exp(t_i/T_{1,2}))^2]$, T was scanned in 400 equal steps in a time range of 20–1000 ms. Uncertainties in the calculated relaxation times were determined in a manner analogous to that described by Stone et al. (1992). The R_1 and R_2 rates used in the present study are those for which the standard deviation to the fitted R_1 and R_2 values was less than 10%.

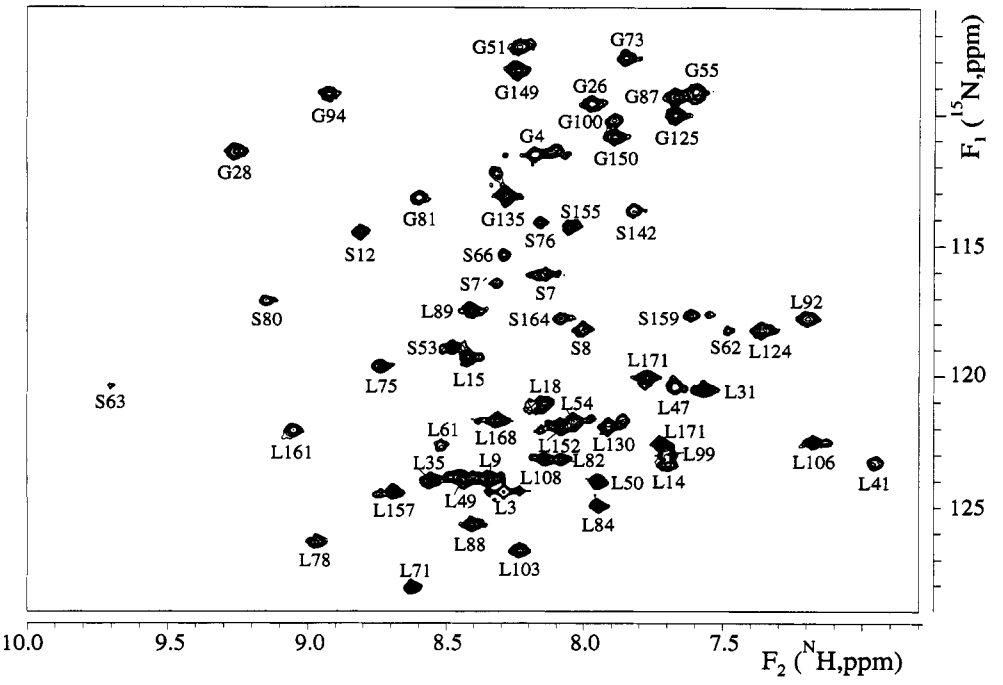

FIGURE 3: HMQC spectrum of residue-specific labeled [^{15}N]Gly,Leu,Ser-rh-metG-CSF.

Assignments. The identification of spin systems could not be achieved with conventional 2D and 3D TOCSY spectra due to the short T_2 relaxation time of the protein. Typical line widths were 30 Hz for a single quantum magnetization of ^{1}H amide protons and 20 Hz for the heteronuclear multiple quantum magnetization of ^{15}N backbone nitrogens in the ^{15}N-labeled samples. This step of the assignment therefore relied on the use of the ^{1}H–^{15}N spectra of residue-specific ^{15}N-labeled rh-metG-CSF samples instead (Muchmore et al., 1989). Six samples were prepared: one each labeled with [^{15}N]Leu, [^{15}N]Gly, [^{15}N]Gly,Ser, [^{15}N]Leu,Gly,Ser, [^{15}N]-Ala, and [^{15}N]Val,Lys. Figures 2 and 3 show the ^{1}H–^{15}N spectra of uniformly ^{15}N-labeled and specifically labeled [^{15}N]-Leu,Gly,Ser-rh-metG-CSF samples. These allowed the identification of 91 (33 leucines, 14 glycines, 14 serines, 19 alanines, 7 valines, and 4 lysines) of the 161 spin systems (175 minus 13 prolines and 1 N-terminal methionine) visible in the ^{1}H–^{15}N spectrum of uniformly labeled rh-metG-CSF. The sequential assignment was carried out using the 3D NOESY–HMQC spectra of both uniformly and specifically ^{15}N-labeled rh-metG-CSF samples (Zink et al., 1992). The HNCA triple-resonance experiment on a uniformly ^{15}N,^{13}C-labeled sample enabled the identification and sequential assignment of residues not located in α-helices. Figure 4 gives a typical example of the HNCA spectrum. The nonhelical residue G135 gives rise to a strong connectivity, whereas for the helix residue G81, only the intraresidue peak can be seen. Table IS summarizes the chemical shifts for the residues assigned (supplementary material).

Interproton Distance Constraints. Sequential NOEs were mainly derived from 3D NOESY–HMQC spectra of uniformly and specifically labeled rh-metG-CSF in H_2O at a mixing time of 90 ms. Long-range NOEs were extracted mainly from 2D NOESY spectra in D_2O and H_2O at mixing times of 40 and 100 ms. The identification of long-range NOEs was difficult due to both the intense overlap of resonances and the small range of chemical shifts as a result of the largely α-helical secondary structure. The 2D NOESY from a deuterated [3,5-$^2H_2$]Phe-rh-metG-CSF sample proved to be crucial in identifying long-range NOEs of aromatic

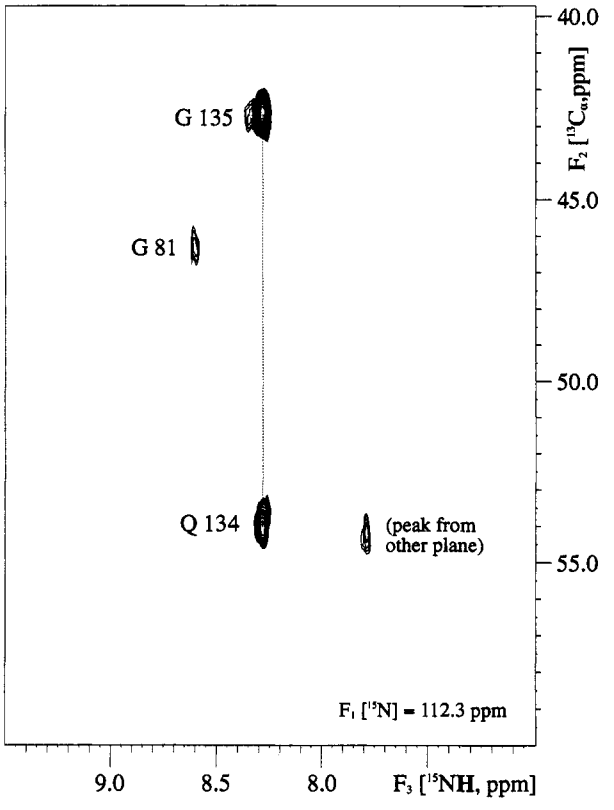

FIGURE 4: Example of a typical $^{13}C(F_2)$–$^1H(F_3)$ plane taken at $^{15}N(F_1)$ = 112.3 ppm through the HNCA spectrum of G-CSF.

protons. A total of 90 long-range NOEs with one connectivity partner being an aromatic proton could be identified. The NOEs were classified into strong, medium, and weak corresponding to distance constraints of 1.8–2.9, 2.0–3.5, and 2.5–5.2 Å, respectively (Williamson et al., 1985; Holak et al., 1989). All protons were explicitly defined in the simulated annealing calculations; additional terms were added to the upper bounds in some cases, however, corresponding to the pseudoatom correction introduced by Wüthrich et al. (1983).

Table 1: Average Deviations from Ideality, Energies of the Structures, and rms Differences between Experimental and Calculated Distance Constraints[a]

parameter	⟨SA⟩	$(SA)_m$
deviations from idealized geometry		
bonds (Å) (2687)	0.006 ± 0.001	0.006
angles (deg) (4892)	0.750 ± 0.015	0.827
impropers (deg) (1368)	0.385 ± 0.039	0.454
energies (kcal mol^{-1})		
F_{NOE}	177 ± 38	220
F_{tor}	0.118 ± 0.040	0.106
F_{repel}	373 ± 15	407
F_{L-J}	−312 ± 23	−208
no. of residual constraint violations (rmsd in Å) for all 778 constraints		
0.2 ≤ rmsd ≤ 0.4	9.2 ± 2.6	10
0.4 < rmsd ≤ 0.5	1.2 ● 1.1	4
>0.5	0	2
rms differences from experimental constraints (Å)		
all (778)	0.075 ± 0.007	0.084
long ($\|i-j\| \geq 5$) (97)	0.050 ± 0.016	0.056
intraresidue (0)		

[a] The ⟨SA⟩ structures are the 20 final structures, $(SA)_m$ is the structure obtained by constrained minimization of the mean structure. The mean structure was obtained by averaging the coordinates of the 20 final ⟨SA⟩ structures best fit to N, C_α, and C atoms of all residues except residues 1–11, 43–70, 93–102, 126–144, and 171–174. The numbers of bond, angle, and improper terms are given in parentheses. The rms deviations (in angstroms) from the interproton distance constraints were calculated as described in Holak et al. (1989). The number of distance constraints is given in parentheses.

Hydrogen Bond Constraints. Hydrogen bond constraints were introduced for those residues in helices that showed NH(i)–NH($i\pm1$) and C$^\alpha$H(i)–NH($i,i+3$) cross peaks and exhibited slowly exchanging NH protons [Figure 3 in Zink et al. (1992)]. There were 64 such hydrogen bonds included in the calculations. Two distance constraints were used for each hydrogen bond: one distance of 1.5–2.3 Å between atoms NH_i and O_{i+4}, and one distance of 2.3–3.3 Å between atoms N_i and O_{i+4}.

Structure Calculations. Structures were calculated with the program X-PLOR (Brünger, 1988; Brünger & Nilges, 1993). Starting structures were produced either by calculating an initial set of substructures incorporating only about one-third of the atoms (followed by simulated annealing with all atoms) (Holak et al., 1989) or by calculating the initial structures in which α-helices were fixed to the standard α-conformation and the rest of the polypeptide chain was in an extended conformation. Starting structures were then subjected to simulated annealing (Nilges et al., 1988). The particular simulated annealing protocol has been described elsewhere (Holak et al., 1989). An iterative approach was employed in the structure calculation, incorporating more experimental constraints at each successive stage. The secondary structure was well defined at all stages of the structure determination. The structures presented in this paper were obtained with the maximum number of NOEs that could be extracted from all NMR spectra acquired in this work (Table 1; a list of NOEs used to determine the structures of G-CSF is included in the supplementary material).

RESULTS

Converged Structures. Superposition of the final structures is shown in Figures 5, and plots of atomic rmsd distributions are shown in Figure 6. From Table 2, it is evident that all SA structures, as well as the average $(SA)_m$ structure, satisfy the experimental constraints, exhibit small deviations from idealized covalent geometry, and have very good nonbonded contacts, as shown by small values of energies and negative Lennard-Jones van der Waals energies. The backbone of rh-metG-CSF within the helices is well determined. The segments of residues 42–47, 60–70, 93–100, and 126–142 show the greatest variability in positions of atoms (Figure 6). This variability may be due in part to a lack of NOEs in most of the residues in these fragments. The average of the rms differences for the backbone atoms in helices among the 20 structures was 1.18 ± 0.45 Å and was 1.62 ± 0.62 Å for all atoms. The corresponding rms difference averages for heavy atoms in the loops were 2.85 ± 1.70 Å for the backbone atoms and 3.34 ± 1.89 Å for all atoms.

Analysis of ^{15}N NMR Relaxation Data. The experimental ^{15}N NOE, T_1, and T_2 values are plotted against amino acid sequence in Figure 6. T_1 values could be determined for 138 of the total 173 residues. The mean T_1 was calculated to be 988 ms, ranging from 720 ms for Ala 6 to 1289 ms for Tyr 39. The mean transverse relaxation time (T_2) of the 123 residues is 99 ms, with a standard deviation of 130 ms. Maximum values were found to be at the N-terminus, with T_2 values up to 1172 ms. Quantitative NOE measurements were possible for 108 residues, with an average value of 0.7.

Amide ^{15}N relaxation was analyzed using standard expressions, assuming dipolar coupling between nitrogen and its attached proton and a contribution from the ^{15}N chemical shift anisotropy (Abragam, 1961; Kay et al., 1989; Clore et al., 1990a,b; Stone et al., 1992). For clarity, we give here the dependence of relaxation parameters on the spectral density function, $J(\omega)$, used in the present study:

$$R_1 = \frac{1}{T_1} = d^2[J(\omega_H - \omega_N) + 3J(\omega_N) + 6J(\omega_N + \omega_H)] + \mathrm{csa}J(\omega_N)$$

$$R_2 = \frac{1}{T_2} = \frac{d^2}{2}[4J(0) + J(\omega_H - \omega_N) + 3J(\omega_N) + 6J(\omega_H) + 6J(\omega_H - \omega_N)] + \frac{\mathrm{csa}}{6}[4J(0) + 3J(\omega_N)] + R_{ex}$$

$$\mathrm{NOE} = 1 + \frac{\gamma_H}{\gamma_N} d^2 T_1 [6J(\omega_H + \omega_N) - J(\omega_H - \omega_N)]$$

where $d^2 = \hbar\gamma_N^2\gamma_H^2/4r_{NH}^6$ and $\mathrm{csa} = (1/3)\omega_N^2(\sigma_\parallel - \sigma_\perp)^2$; $\hbar$ is Planck's constant, γ_H and γ_N are the gyromagnetic ratios of ^1H and ^{15}N, respectively, $r_{NH} = 1.02$ Å is the mean nitrogen–hydrogen bond length, ω_N and ω_H are the corresponding Larmour frequencies, and $(\sigma_\parallel - \sigma_\perp)$ is the difference between the parallel and perpendicular components of the chemical shift tensor, which was set to −160 ppm (Hiyama et al., 1988). An additional term, R_{ex}, was introduced in the expression for T_2 to account for conformational averaging and/or amide exchange effects on a microsecond to millisecond time scale.

A total of 94 amide protons, for which NOE, T_1, and T_2 could be measured simultaneously, were used in the analysis of the relaxation data based on the model-free formalism of Lipari and Szabo (1982a,b) with parameters τ_m, τ_e, S^2, and R_{ex} (see eqs below). The following target function was minimized, $F_{error} = [((R_{1,obs} - R_{1,calc})/R_{1,obs})^2 + ((R_{2,obs} - R_{2,calc})/R_{2,obs})^2 + (NOE_{obs} - NOE_{calc})^2]^{1/2}$, for each residue separately, where $R_{1,obs}$, $R_{2,obs}$, and NOE_{obs} are the experimental values of relaxation rates and NOEs, respectively, and $R_{1,calc}$, $R_{2,calc}$, and NOE_{calc} are the values calculated with the equations given above. A Monte Carlo minimization of this target function was carried out with parameters τ_e, S^2,

FIGURE 5: Stereoview of the backbone atoms (N, C_α, C, and O) of 10 solution structures of rh-metG-CSF fitted to the N, C_α, C, and O of all residues except 1–10, 43–70, 93–101, 125–143, and 171–174. The N-terminus is located in the lower right corner.

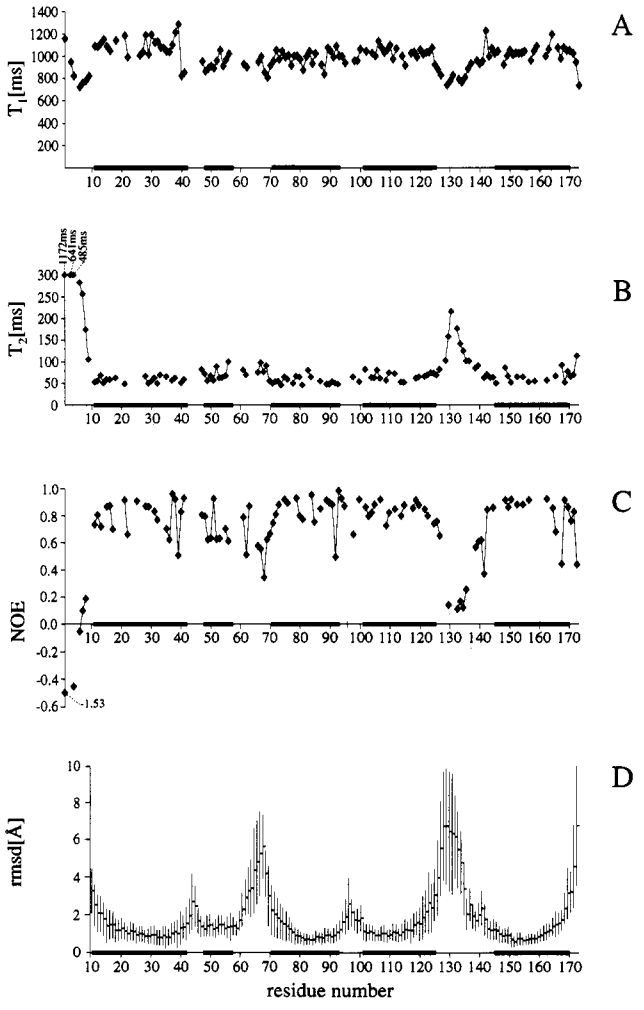

FIGURE 6: Experimental relaxation parameters (A) ^{15}N T_1, (B) ^{15}N T_2, and (C) ^{15}N NOE and (D) rmsd values for the final solution structures of rh-metG-CSF. For the calculation of the rmsd values, 20 NMR structures were fit to residues 11–42, 71–92, 102–124, and 144–170 of their minimized mean structure.

and R_{ex}. The global error minimization, ΣF_{error}, as carried out in Stone et al. (1992), was not performed since a few "problematic" data points can dominate such a sum of the squared residuals, whereas for most residues the error was low over a long span of τ_m's.

Table 2: rms Differences between (A) 20 NMR Solution Structures and Their Minimized Mean, (B) 20 NMR Solution Structures and the X-ray Structure, and (C) the Minimized Mean of 20 NMR Solution Structures and the X-ray Structure of G-CSF

	rmsd (Å)
(A)	
backbone atoms of helices A–D[a]	1.18 ± 0.45
all heavy atoms of helices A–D[a]	1.62 ± 0.62
backbone atoms of loops AB, BC, and CD[b]	2.85 ± 1.70
all heavy atoms of loops AB, BC, and CD[b]	3.34 ± 1.89
(B)	
backbone atoms of helices A–D[a]	2.95 ± 1.75
all heavy atoms of helices A–D[a]	3.44 ± 1.89
(C)	
backbone atoms of helices A–D[a]	2.86
all heavy atoms of helices A–D[a]	3.33
backbone atoms of all residues present in X-ray structure[c]	3.15
all heavy atoms of all residues present in X-ray structure[c]	3.70

[a] Helix A, residues 11–41; helix B, residues 71–95; helix C, residues 103–125; helix D, residues 145–171. [b] Loop AB, residues 42–70; loop BC, residues 96–102; loop CD, residues 126–144. [c] Residues 10–62, residues 72–127, and residues 138–172. The N-terminal residues 1–9 and the C-terminal residues 172–175 were neglected.

Initial Estimation of the Overall Rotational Correlation Time. For a spherical molecule, the spectral density function is

$$J(\omega) = \frac{2}{5}\left[\frac{S^2\tau_m}{1+(\omega\tau_m)^2} + \frac{(1-S^2)\tau}{1+(\omega\tau)^2}\right]$$

where $1/\tau = 1/\tau_m + 1/\tau_e$. For proteins that are assumed to have a roughly spherical shape, an initial estimate of the overall rotational correlation time, τ_m, could be obtained from the T_1/T_2 ratios for residues in structurally well-defined segments that do not show evidence of line-width broadening from the R_{ex} effects. If a certain (and small) degree of anisotropy is present, τ_m can still be estimated using the precedure of Barbato et al. (1993). This procedure assumes that anisotropy should have a small effect on the relaxation parameters, with the exception of residues for which $(T_{2,i} - \langle T_2\rangle)/T_{2,i} > 3(\langle T_1\rangle - T_{1,i})/T_{1,i}$, where $\langle T_{1,2}\rangle$ are the average relaxation times.

The average $\langle T_2 \rangle$ of G-CSF was calculated by taking into account the T_2 values smaller than 100 ms and not, as in Barbato et al. (1993), the T_2's of all residues. Although our approach allowed for more residues that would be considered "anisotropic" to be excluded, there were in fact few such residues in G-CSF (Figure 6a–c).

In G-CSF, the average T_1/T_2 ratio was determined to be 16.2 for residues in well-defined helical regions that had NOE > 0.7. From the total of 94 residues for which NOE, T_1, and T_2 were determined simultaneously, 49 residues had NOEs larger than 0.7. Using 33 residues that had a T_1/T_2 ratio within one standard devation of the average T_1/T_2 ratio, the average calculated τ_m was 12.1 ns. Similar results were obtained when all residues that display NOE > 0.75 (60, which were all also nonhelical) were considered. The T_1/T_2 ratio for G-CSF is much higher (by a factor of 1.5–3.0) than those reported for proteins for which ^{15}N relaxation data have been reported to date (Kay et al., 1989; Clore et al., 1990a; Barbato et al., 1992; Berglund et al., 1992; Kördel et al., 1992; Redfield et al., 1992; Stone et al., 1992; Schneider et al., 1992; Cheng et al., 1993). Such a high ratio may indicate that modeling of the relaxation data with the extended Lipari–Szabo model (Lipari & Szabo, 1982a,b; Clore et al., 1990a,b; Palmer et al., 1991; Stone et al., 1992) requires analysis of the spectral density function, with the addition of conformational exchange broadening in the expression for T_2 for almost *all* residues. The short T_2 values could also be due to a longer effective rotational correlation time of G-CSF due to its aggregation.

The relaxation data, in principle, could be fit using a model with relatively short τ_m's (5–8 ns) and large contributions from the microsecond-to-millisecond time scale transitions (R_{ex}) or a model that uses longer τ_m's (10–17 ns) and a small contribution from R_{ex}. We therefore developed a more general method for determining τ_m. The procedure is iterative and self-consistent, producing the best optimized τ_m compatible with the available relaxation data. The T_1/T_2 ratios for the well-defined helical regions were used to determine the initial range of τ_m with the exchange parameter R_{ex} set to 0. There were 89 such residues from the total 123 residues for which T_1 and T_2 could be determined simultaneously. The average calculated τ_m was 13 ± 4 ns. For each integer value of the τ_m between 9 and 17 ns, the relaxation data were fit using full equations for T_1, T_2 (including R_{ex}), and NOE. In the next step, only residues with a maximum value of 10% contribution from R_{ex} to the time rate $1/T_2$ were retained. Using the relaxation times of these selected residues, the overall correlation time τ_m was calculated assuming $R_{ex} = 0$. There were, for example, only 5 residues that fulfilled this condition for $\tau_m = 10$ ns and 59 residues for $\tau_m = 17$ ns. These calculated average τ_m's were then plotted against the initial input τ_m's (Figure 7). The optimized τ_m was determined to be 12 ns, as this value gave the minimum difference between input and calculated correlation times.

Anisotropy of Molecular Motion. The shape of the G-CSF molecule clearly is not spherical, and therefore some degree of anisotropy should be considered in the interpretation of the relaxation data. Indeed, some patterns in the T_1 and T_2 values seen in Figure 6 could be ascribed as originating from the anistropic motion of the G-CSF molecule. Motional anisotropy affects the observed T_1 and T_2 values in opposite ways (Woessner et al., 1962; Woessner, 1960; Huntress, 1968; Hubbard, 1970). Such a trend can be observed in T_1 and T_2 for residues 127–136 (Figure 6).

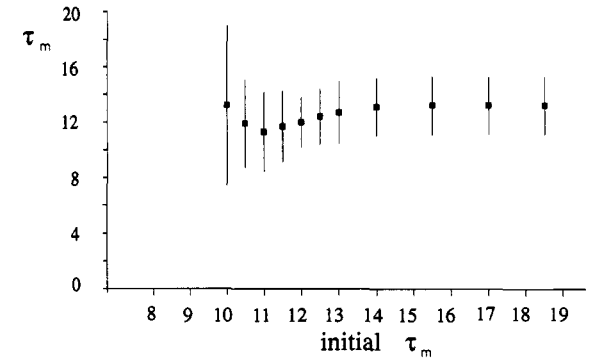

FIGURE 7: Plot of calculated correlation times τ_m derived from the optimization of relaxation parameters vs initial correlation times τ_m used as input for the calculation of relaxation parameters.

For anisotropic motion, the total correlation function was approximated by an equation for an axially symmetric molecule (Woessner et al., 1962; Woessner, 1960; Huntress, 1968; Hubbard, 1970), in which internal motion was assumed to be much faster than the overall motion, and for which the internal motion was in the extreme narrowing limit ($(\omega\tau_e)^2 \ll 1$):

$$J(\omega) = \frac{2}{5}S^2\left[\frac{A_1\tau_1}{1+(\omega\tau_1)^2} + \frac{A_2\tau_2}{1+(\omega\tau_2)^2} + \frac{A_3\tau_3}{1+(\omega\tau_3)^2}\right] + \frac{2}{5}\frac{(1-S^2)\tau}{1+(\omega\tau)^2}$$

where $A_1 = 0.75 \sin^4\alpha$, $A_2 = 3\sin^2\alpha\cos^2\alpha$, and $A_3 = (1.5\cos^2\alpha - 0.5)^2$, with α being the angle between the NH–N bond vector and the long axis of the molecule. τ is given by $1/\tau = 1/\tau_e + 1/\tau_{c,eff}$, with an average overall correlation time, $\tau_{c,eff}$, approximated by $\tau_{c,eff} = (4D_\perp + 2D_\parallel)^{-1}$ (the second term in the equation for $1/\tau$, $1/\tau_{c,eff}$, is actually residue dependent on α; however, since this term has only a negligible contribution to $1/\tau$ and the anisotropy of the molecule is not high, the use of an average correlation time $\tau_{c,eff}$ over all residues is sufficient). The three rotational correlation times for anisotropic motion, τ_1, τ_2, and τ_3, are given by $\tau_1 = (4D_\parallel + 2D_\perp)^{-1}$, $\tau_2 = (D_\parallel + 5D_\perp)^{-1}$, $\tau_3 = (6D_\perp)^{-1}$

The degree of anisotropy of a molecule of length a and diameter b can be described by a factor σ:

$$\sigma = \frac{D_\parallel}{D_\perp} = \left[\frac{1-\rho^4}{(2-\rho^2)G-2}\right]\left[\frac{\rho^2(1-\rho^2)}{2-\rho^2 G}\right]^{-1}$$

with

$$G = 2a(a^2-b^2)^{-1/2}\ln\left[\frac{a+(a^2-b^2)^{1/2}}{b}\right]; \quad \rho = b/a,\ a > b$$

The anisotropy of the G-CSF molecule was determined from coordinates of the average NMR structure, taking into account N atoms only. The three-dimensional covariance matrix of the N coordinates was constructed, and the eigenvector of the highest eigenvalue of this matrix was assumed to be the long axis of the molecule. The direction angle α of the N–NH bonds was then referenced to this axis. Angle α was 20° (or 160°) ± 20° for helices and 90° ± 30° for loops. The eigenvalues of the covariance matrix were 1.00:1.25:4.84. The molecule of G-CSF was approximated by a symmetric ellipsoid with axes 26, 26, and 45 Å. As described by Woessner et al. (1962), the two diffusion constants $D_\perp$ and $D_\parallel$ for a symmetric ellipsoid with one long axis are related by factor σ defined above in equations describing the shape of the molecule. For

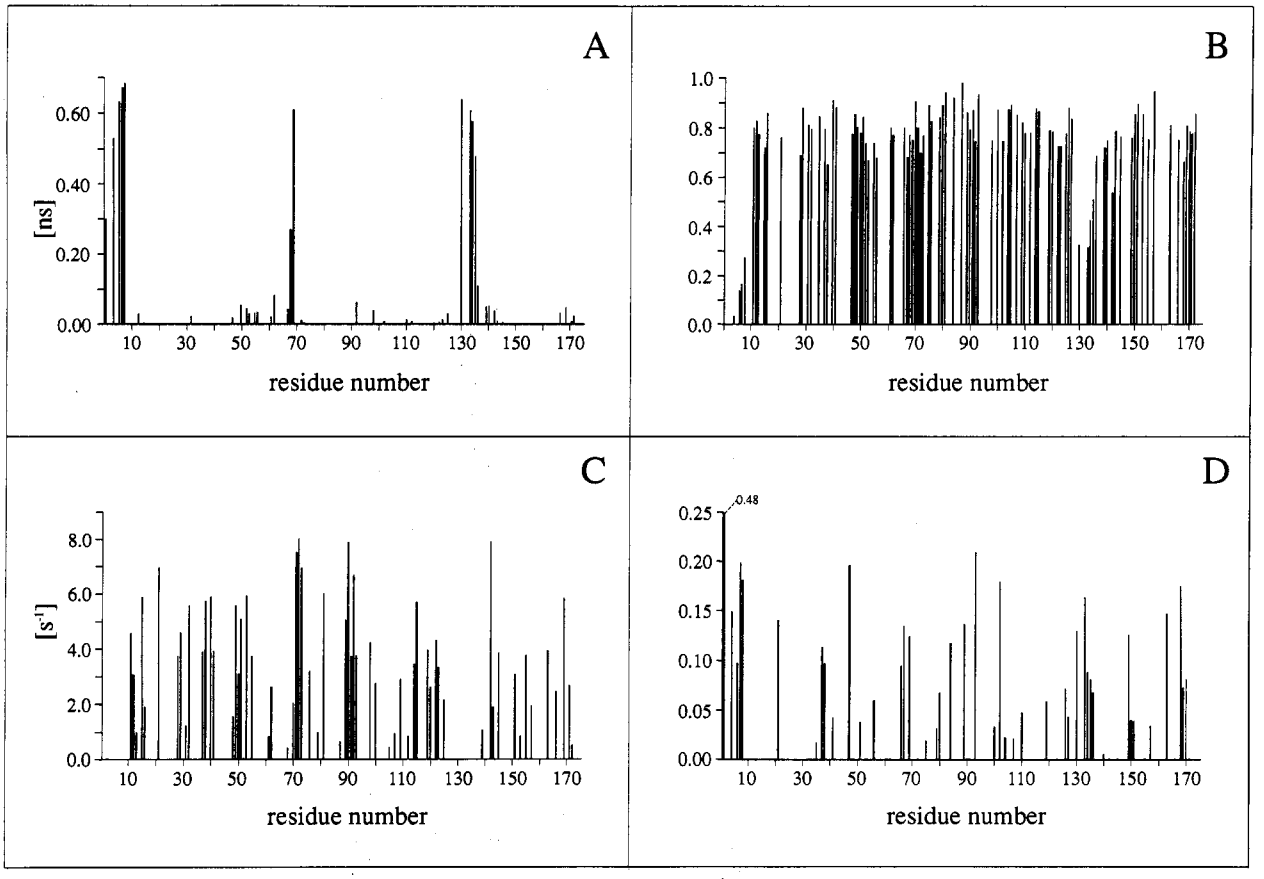

FIGURE 8: Calculated relaxation parameters for rh-metG-CSF for a correlation time τ_3 = 13 ns and σ^{-1} = 0.62 vs amino acid sequence: (A) internal correlation time, τ_e, values plotted only for residues with $S^2 < 0.75$; (B) order parameter S^2; (C) chemical exchange parameter R_{ex}; (D) error fit function F_{error} (see text).

easier comparison with the isotropic model, the longest of the three correlation times, τ_3, and σ were used as input for fitting τ_e, S^2, and R_{ex} in the anisotropic model. The correlation time τ_3 was set to integer numbers between 9 and 15 ns. For G-CSF, σ^{-1} was determined to be 0.62, and the data for this value and for τ_3 = 13 ns are shown here, as τ_3 = 13 ns gave the smallest error of the fit of the relaxation data. However, since G-CSF is not exactly an ellipsoid, σ^{-1} values of 0.4, 0.5, 0.6, 0.7, and 0.8 were also tested and gave results similar to that of σ^{-1} = 0.62 (supplementary material).

Presence of Fast Internal Motions in Loops. Plots of the generalized order parameter S^2, R_{ex}, τ_e, and a fit error F_{error} as a function of the amino acid sequence are shown in Figure 8. Both the isotropic (supplementary material) and anisotropic models indicate a high mobility of certain loop regions of G-CSF. An average order parameter S^2 is on the order of 0.74 for all residues. For the 55 residues in the loop regions, the mean S^2 reduces to 0.57, indicating fast motion of the NH bond vector. These are described further through the internal correlation time τ_e, which has an average of 0.42 ns in these regions.

The relaxation data of G-CSF were also fit to a model that assumed that G-CSF was a rigid and highly anisotropic molecule with no fast internal motion. σ^{-1} values between 0.4 and 0.01 were tested (data not shown). The error of the fit of the relaxation parameters, F_{error}, was on average 200%, indicating that the anisotropy itself could not account for the relaxation data. Even for a physically unrealistically high anisotropy of σ^{-1} equal to 0.01, the error, F_{error}, was on average 150%, with the loops having values of 200% (see the supplementary material). High values of F_{error} arise because the anistropic model cannot account for the observed NOE data. Although for molecules undergoing anisotropic motion NOE is α dependent, the influence of anisotropy on the NOEs is small; for example, the NOE changes 2% for α values between 60–90° for a model of G-CSF that assumes σ^{-1} = 0.01. On the other hand, NOEs are sensitive to the effective correlation time of the fast internal motion. Thus, the present study unequivocally shows that there is a high degree mobility for residues in the loop connecting helices C and D.

DISCUSSION

rh-metG-CSF consists of a four-helix-bundle fold (Figures 5 and 9). An additional short helix is part of the first long loop connecting helices A and B. This helix (E) is perpendicular to the main axis defined by the four-helix bundle. The long AB loop from residues 42 to 69 allows helices A and B to be aligned parallel rather than antiparallel in the structure. The same holds true for helices C and D, which are connected by a long CD loop from residues 126 to 144. This results in an up–up–down–down alignment of the four major helices (Figures 5 and 9). The two disulfide bridges in rh-metG-CSF both occur in the long AB loop; at the C-terminus of helix A (Cys 36–Cys 42) and the N-terminus of helix B (Cys 64–Cys 74). These disulfide bridges are essential for the biological activity of G-CSF (Lu et al., 1992).

The global fold of G-CSF is reasonably well defined, as the long-range NOE constraints that established the global fold, although few in number, were favorably distributed throughout the peptide sequence. The present study shows that the three-dimensional fold of a large, mostly α-helical protein can be defined from backbone NOE constraints (obtained from ^{15}N-edited spectra) and from constraints involving aromatic

FIGURE 9: Ribbon plot of rh-metG-CSF. The N-terminus is located in the lower right corner.

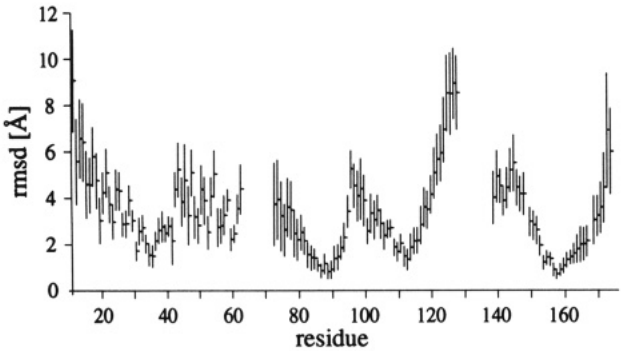

FIGURE 10: rms difference between 20 NMR structures and the X-ray structure of G-CSF.

residues. Our results also indicate the relatively low limit of precision in such structures, when no additional constraints from the 3D and 4D NMR spectra of ^{13}C,^{15}N-labeled protein are available, particularly for side chains. In the case of this predominantly helical protein, with its regular and rather uncomplicated topology, the global fold was successfully established from limited NOE data. This might not be the case for β-strand proteins: backbone distance constraints were insufficient to correctly calculate the polypeptide fold of the *Bacillus subtilis* glucose permease IIA domain (Fairbrother et al., 1992).

At the same time that the NMR structural determination was completed, the results of an independently determined X-ray structure of G-CSF were published (Hill et al., 1993). Figure 10 shows a residue-specific rmsd between 20 individual NMR structures and the crystal structure. Superposition of the average NMR structure with the X-ray structure is shown in Figure 11. The overall folds obtained by the X-ray and NMR methods are very similar. The crystal structure has an *R* factor of 21.5% for all data between 6.0- and 2.2-Å resolution. Ten residues at the N-terminus and parts of the loops (63–71 and 128–137) are not identified in the crystal structure; in addition, residues 147 and 166 in helix D are

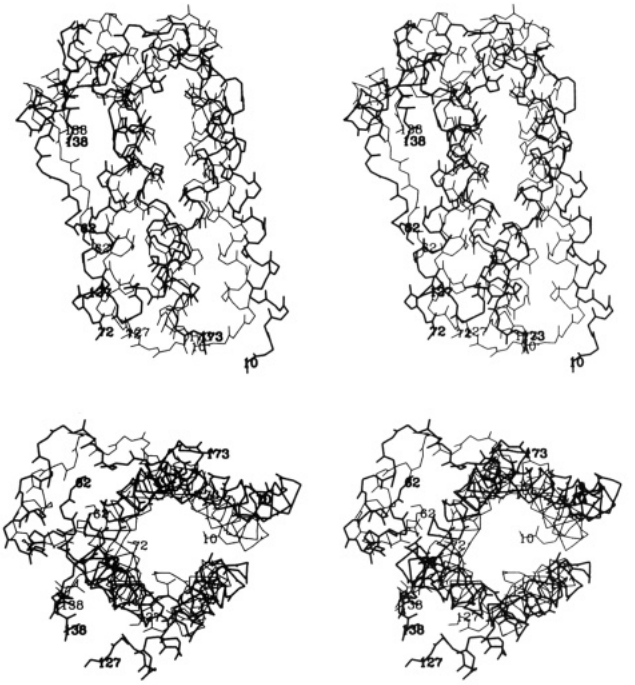

FIGURE 11: Overlay stereoplot of the X-ray structure (thin line) (Hill et al., 1993) and the average of 20 NMR solution structures (thick line) of rh-metG-CSF. The structures were fit to residues 14–40, 74–90, 105–121, and 147–167 of helices A–D. For clarity, residue numbers are given for the first and last residues of each segment shown. Top: View is identical to that in Figure 5. Bottom: View along the helix-bundle main axis. For the NMR structure, only segments of the polypeptide chain that are also present in the X-ray structure are shown.

replaced by alanines. The loop segments missing from the X-ray structure exhibit the highest variability of the backbone in the NMR structures. rmsd values between the minimized means of 20 NMR structures and the crystal structure are 2.8 Å for backbone atoms and 3.3 Å for all non-hydrogen atoms if only helices are considered (Table 2). These relatively large rms differences can be attributed to the rather low resolution of the NMR structure; thus, delineation of genuine differences between solution and crystal structures is not possible at present. A substantial number of additional long-range NOEs could, however, be assigned in the NMR spectra on the basis of the interproton distances derived from the coordinates of the X-ray structure. The presence of these additional NOEs provides further proof that the solution and crystal structures are similar. Inclusion of the NOEs derived from the X-ray structures improved the precision of the NMR structure considerably (data not shown); these were not used in the calculation of structures in Figure 5, however.

The ^{15}N relaxation data of G-CSF show that loop regions (and a few residues at the N- and C-termini) are more flexible than the helical core region of the protein. Particularly striking are the small NOE and long T_2 values for many residues in the loop between helices C and D. These residues therefore exhibit a significant degree of rapid motion in the protein backbone compared with the overall rotational correlation time of the whole molecule. The overall correlation time τ_m in the isotropic model of G-CSF was optimized to be 12.1 ns (and 13 ns in the anisotropic model). The overall τ_m of G-CSF is larger than those for other ~18-kDa proteins: staphylococcal nuclease, 9.1 ns at 35 °C (Kay et al., 1989); interleukin-1β, 8.3 ns at 36 °C (Clore et al., 1990a); and glucose permease IIA domain of *Bacillus subtilis*, 6.2 ns at 35 °C (Stone et al., 1992). This difference is most probably due to the lower

temperature used in the NMR measurements of G-CSF and to the aggregation of G-CSF (cf. Materials and Methods)

Generally, there seems to be no significant chemical or conformational exchange within loops, as the average R_{ex} is 0.74 s^{-1} compared to an overall mean value of 1.78. The 114 residues in helical regions have an average order parameter value of 0.84. The average value of the NOEs is 0.83. These values indicate that most of the helical backbones exist in well-defined structures of limited conformational flexibility (on the nanosecond-to-picosecond time scale), with no motion faster (picosecond time scale) than τ_m of small magnitude. Although motions on the picosecond time scale appear relatively restricted throughout most of the helices, relaxation data indicate that motions on the millisecond-to-microsecond time scale (R_{ex}) are found in many helical residues. Here the exchange parameter increases to 7.92 for Leu 92, leading to an average of 2.32.

The rmsd values for the backbone heavy atoms for the calculated structures are shown in Figure 6. It is clear that there is a correlation between these values and the T_2 and NOE values. This is translated into the correlation between rmsd's and the S^2 values (Figure 8). The observation of long T_2, small NOE, and low S^2 values for loop CD suggests that the poor definition of these regions in the calculated NMR structures arises from the dynamic behavior in this segment, which in turn causes the paucity of the assigned NOEs in these regions.

The dynamical behavior of G-CSF should be compared to a recent analysis of the relaxation data of interleukin-4 (Redfield et al., 1992). The helical core of this four-helix-bundle protein exists as a well-defined structure of limited conformational flexibility ($S^2 \approx 0.9$), whereas two loops of the three joining the helices experience substantial fluctuations in the main-chain conformation ($S^2 \approx 0.2$–0.8). In G-CSF, such behavior is observed for all helices and loop CD. Thus, the dynamic properties observed here might be general for this class of proteins and may be significant for the interpretation of both their structural and functional properties.

ACKNOWLEDGMENT

We are most grateful to Milton Stubbs for helpful discussions and David Eisenberg for the coordinates of the crystal structure of G-CSF.

SUPPLEMENTARY MATERIAL AVAILABLE

The supplementary material includes a table of the ^1H, ^{13}C, and ^{15}N assignments; a list of NOEs used to determine structures of G-CSF; and a table containing experimental data for T_1 and T_2 relaxation times and NOEs, along with calculated S^2, τ_m, τ_e, τ_3, and R_{ex} for various models of isotropic and anisotropic molecular motions (55 pages). Ordering information is given on any current masthead page.

REFERENCES

Barbato, G., Ikura, M., Kay, L. E., Pastor, R. W., & Bax, A. (1992) *Biochemistry 31*, 5269–5278.

Bax, A., & Davis, D. G. (1985) *J. Magn. Reson. 65*, 355–366.

Bax, A., & Grzesiek, S. (1993) *Acc. Chem. Res. 26*, 131–138.

Bazan, J. F. (1991) *Neuron 7*, 197–208.

Bodenhausen, G., Kogler, H., & Ernst, R. R. (1984) *J. Magn. Reson. 58*, 370–380.

Boyd, J., Hommel, U., & Campbell, I. D. (1990) *Chem. Phys. Lett. 175*, 477–482.

Brünger, A. T. (1988) *J. Mol. Biol. 203*, 803–816.

Brünger, A. T., & Nilges, M. (1993) *Q. Rev. Biophys. 26*, 49–125.

Bundi, A., & Wüthrich, K. (1979) *Biopolymers 18*, 285–312.

Cieslar, C., Ross, A., Zink, T., & Holak, T. A. (1993) *J. Magn. Reson. B 101*, 97–101.

Clark, S. C., & Kamen, R. (1987) *Science 236*, 1229–1237.

Clore, G. M., Driscoll, P. C., Wingfield, P. T., & Gronenborn, A. M. (1990a) *Biochemistry 29*, 7387–7401.

Clore, G. M., Szabo, A., Bax, A., Kay, L., Driscoll, P. C., & Gronenborn, A. M. (1990b) *J. Am. Chem. Soc. 112*, 4989–4991.

Clubb, R. T., Thanabal, V., & Wagner, G. (1992) *J. Biomol. Nucl. Magn. Reson. 2*, 203–210.

Constantine, K. L., Friedrichs, M. S., Goldfarb, V., Jeffrey, P. D., Sheriff, S., & Mueller, L. (1993) *Proteins 15*, 290–311.

Crawford, J., Ozer, H., & Johnson, D. (1990) *Proc. Am. Soc. Clin. Oncol. 9*, A884.

Davis, D. G., & Bax, A. (1985) *J. Am. Chem. Soc. 107*, 2820–2821.

De Vos, A. M., Ultsch, M., & Kossiakoff, A. A. (1992) *Science 255*, 306–312.

Diederichs, K., Boone, T., & Karplus, P. A. (1991) *Science 254*, 1779–1782.

Ernst, R. R., Bodenhausen G., & Wokaun, A. (1987) *Principles of Nuclear Magnetic Resonance in One and Two Dimensions*, Clarendon Press, Oxford, U.K.

Fairbrother, W. J., Gippert, G. P., Reizer, J., Saier, M. H., Jr., & Wright, P. E. (1992) *FEBS Lett. 296*, 148–152.

Fesik, S. W., & Zuiderweg, E. R. P. (1990) *Q. Rev. Biophys. 23*, 97–131.

Freund, C., Ross, A., Plückthun, A., & Holak, T. A. (1994) *Biochemistry 33*, 3296–3303.

Gabrilove, J. L. (1992) *Growth Factors 6*, 187–191.

Glaspy, J. A., & Golde, D. W. (1992) *Sem. Oncol. 19*, 386–394.

Glaspy, J. A., Moreno, J., & Mitsujasu, R. (1989) *Mol. Biother. 1* (Suppl. 17).

Griesinger, C., Sørensen, O. W., & Ernst, R. R. (1987) *J. Magn. Reson. 75*, 474–492.

Griesinger, C., Otting, G., Wüthrich, K., & Ernst, R. R. (1988) *J. Am. Chem. Soc. 110*, 7870–7872.

Habazettl, J., Gondol, D., Wiltscheck, R., Otlewski, J., Schleicher, M., & Holak, T. A. (1992) *Nature 359*, 855–858.

Havel, T. F., & Wüthrich, K. (1985) *J. Mol. Biol. 182*, 281–294.

Hill, C. P., Osslund, T. D., & Eisenberg, D. (1993) *Proc. Natl. Acad. Sci. 90*, 5167–5171.

Holak, T. A., Gondol, D., Otlewski, J., & Wilusz, T. (1989) *J. Mol. Biol. 210*, 635–648.

Ikura, M., Kay, L. E., & Bax, A. (1990) *Biochemistry 29*, 4659–4667.

Kaushansky, K. (1992) *Proteins: Struct., Funct., Genet. 12*, 1–9.

Kay, L. E., Torchia, D. A., & Bax, A. (1989) *Biochemistry 28*, 8972–8979.

Kay, L. E., Ikura, M., Tschudin, R., & Bax, A. (1990) J. Magn. Reson. 89, 496–514.

Kay, L. E., Nicholsons, L. K., Delagrio, F., Bax, A., & Torchia, D. A. (1992) *J. Magn. Reson. 97*, 359–375.

Kirchner, H., Kruse, A., Neustock, P., & Rink, L. (1993) in *Cytokine und Interferone*, pp 32–34 and 126, Spektrum Verlag, Heidelberg.

Kline, A., Braun, W., & Wüthrich, K. (1988) *J. Mol. Biol. 204*, 657–724.

Kubota, N., Orita T., Hattori K., Oheda M., Ochi N., & Yamazaki T. (1990) *J. Biochem. (Tokyo) 107*, 486–492.

Lipari, G., & Szabo, A. (1982a) *J. Am. Chem. Soc. 104*, 4546–4559.

Lipari, G., & Szabo, A. (1982b) *J. Am. Chem. Soc. 104*, 4559–4570.

Lu, H. S., Clogston, C. N., Narhi, L. O., Merewether, L. A., Pearl, W. R., & Boone, T. C. (1992) *J. Biol. Chem. 267*, 8770–8777.

Marion, D., & Wüthrich, K. (1983) *Biochem. Biophys. Res. Commun. 113*, 967–974.

Marion, D., Driscoll, P. C., Kay, L. E., Wingfield, P. T., Bax, A., Gronenborn, A. M., & Clore, G. M. (1989) *Biochemistry 28*, 6150–6153.
McIntosh, L. P., & Dahlquist, F. W. (1990) *Q. Rev. Biophys. 23*, 1–38.
McKay, D. B. (1992) *Science 257*, 412–413.
Messerle, B. A., Wider, G., Otting, G., Weber, C., &. Wüthrich, K. (1989) *J. Magn. Reson. 85*, 608–613.
Metcalf, D. (1986) *Blood 67*, 257–267.
Metcalf, D., & Nicola, N. A. (1983) *J. Cell. Physiol. 116*, 198–206.
Molineux, G., Pojda, Z., Hampson, I. N., Lord, B. I., & Dexter T. M. (1990) *Blood 76*, 2153–2158.
Montelione, G., & Wagner, G. (1990) *J. Magn. Reson. 87*, 183–188.
Morstyn, G., & Burgess, A. W. (1988) *Cancer Res. 48*, 5624–5637.
Muchmore, D. C., McIntosh, L. P., Russell, C. B., Anderson, D. E., & Dahlquist, F. W. (1989) *Methods Enzymol. 177*, 44–73.
Nagata, S. (1989) *BioEssays 10*, 113–116.
Nomura, H., Imazeki, I., Oheda, M., Kubota, N., Tamura, M., Ono, M., Ueyama, Y., & Asano, S. (1986) *EMBO J. 5*, 871–876.
Oheda, M., Hasegawa, M., Hattori, K., Kuboniwa, H., Kojima, T., Orita, T., Tomonou, K., Yamazaki, T., & Ochi, N. (1990) *J. Biol. Chem 265*, 11432–11435.
Palmer, A. G., Skelton, N. J., Chazin, W. J., Wright, P. E., & Rance, M. (1992) *Mol. Phys. 75*, 699–711.
Pandit, J., Bohm, A., Jancarik, J., Halenbeck, R., Koths, K., & Kim, S. H. (1992) *Science 258* (5086), 1358–1362.
Pardi, A., Billeter, M., & Wüthrich, K. (1984) *J. Mol. Biol. 180*, 741–751.
Plateau, P., & Gueron, M. (1982) *J. Am. Chem. Soc. 104*, 7310–7311.
Powers, R., Garrett, D. S., March, C. J., Frieden, E. A., Gronenborn, A. M., & Clore, G. M. (1992) *Science 256* (5064), 1673–1677.
Rance, M. (1987) *J. Magn. Reson. 74*, 557.
Redfield, C., Boyd, J., Smith, L. J., Smith, R. A. G., & Dobson, C. M. (1992) *Biochemistry 31*, 10431–10437.
Riesenberg, D., Menzel, K., Schulz, V., Schumann, K., Veith, G., Zuber, G., & Knorre, W. A. (1990) *Appl. Microbiol. Biotechnol. 34*, 77–82.
Ross, A., Czisch, M., Zink, T., & Holak, T. A. (1993a) *J. Magn. Reson. B* (in press).
Ross, A., Czisch, M., Cieslar, C., & Holak, T. A. (1993b) *J. Biomol. Nucl. Magn. Reson. 3*, 215–224.
Rudolph, R. (1990) in *Modern Methods in Protein and Nucleic Acid Research* (Tschesche, H., Ed.) pp 496–514, Walter de Gruyter, Berlin.
Rudolph, R., et al. (1990) United States Patent 4,933,434.
Scarffe, J. H., & Kamthan, A. (1990) *Cancer Surveys 9*, 115–130.
Seip, S., Balbach, J., & Kessler, H. (1992) *J. Magn. Reson. 100*, 406–410.
Senn, H., Eugster, G., Otting, G., Suter, F., & Wüthrich, K. (1987) *Eur. Biophys. J. 14*, 301–306.
Shaka, A. J., Barker, P. B., & Freeman, R. (1983) *J. Magn. Reson. 64*, 547–552.
Smith, L. J., Redfield, C., Boyd, J., Lawrence, J. M. P., Edwards, R. G., Smith, R. A. G., & Dobson, C. M. (1992) *J. Mol. Biol. 224* (4), 899–904.
Souza, L. M., Boone, T. C., Gabrilove, J., Lai, P., Zsebo, K. M., Murdock, D. C., Chazin, V. R., Bruszewski, J., Lu, H., Chen, K. K., Barendt, J., Platzer, E., Moore, M. A. S., Mertelsmann, R., & Welte, K. (1986) *Science 232*, 61–65.
Stanley, E. R., & Heard, P. M. (1977) *J. Biol. Chem. 252*, 4305–4312.
Stone, M. J., Fairbrother, W. J., Palmer, A. G., III, Reizer, J., Saier, M. H., Jr., & Wright, P. E. (1992) *Biochemistry 31*, 4394–4406.
Summers, M. F., Marzilli, L. G., & Bax, A. (1986) *J. Am. Chem. Soc. 108*, 4285–4294.
Walter, M. R., Cook, W. J., Zhao B. G., Cameron, R. P., Jr., Ealick, S. E., Walter, R. L., Jr., Reichert, P., Nagabhushan, T. L., Trotta, P. P., & Bugg, C. E. (1992) *J. Biol. Chem. 267* (28), 20371–20376.
Williamson, M. P., Havel, T. F., & Wüthrich, K. (1985) *J. Mol. Biol. 182*, 295–315.
Wishart, D. S., Sykes, B. D., & Richards, F. M. (1991) *J. Mol. Biol. 222*, 311–333.
Wüthrich, K. (1986) *NMR of Proteins and Nucleic Acids*, J. Wiley, New York.
Wüthrich, K., Billeter, M., & Braun, W. (1983) *J. Mol. Biol. 169*, 949–961.
Zink, T., Ross, A., Ambrosius, D., Rudolph, R., & Holak, T. A. (1992) *FEBS 314*, 435–439.